Egyptian Journal of Radiology and Nuclear Medicine

RESEARCH

Open Access

The additive diagnostic role of diffusion-weighted magnetic resonance and chemical shift imaging (CSI) in differentiation between malignant and benign cervical lymph nodes

Lamya Eissa[1*], Maged Manosur[1] and Reda Darweesh[1]

Abstract

Background Imaging with conventional MRI plays a pivotal role in differentiation between benign and malignant nodes, which is crucial for choice of therapeutic plan. The purpose of this study was to evaluate the role of diffusion-weighted imaging DWI MRI and chemical shift imaging (CSI) (in and out of phase) in differentiation between malignant and benign cervical lymph nodes.

Patients and methods We prospectively reviewed MR images of 31 patients presented to ENT department by cervical adenopathy. Imaging parameters documented included: morphology, ADC values and in-phase to out-of-phase (Ip/Op) ratios and signal drop in out-of-phase images.

Results ADC values of the benign and malignant nodes were 1.06 ± 0.25 and 0.85 ± 0.24, respectively. A statistically significant difference was found between the two groups ($p = 0.041$). An ADC value of 0.9×10^{-3} mm^2/s was concluded to be the best cutoff value for differentiating benign from malignant LNs. The mean values of in/out-of-phase ratios of benign and malignant lymph nodes were 0.75 ± 0.16 and 0.96 ± 0.06, respectively. A statistically significant difference was found between the two groups ($p = 0.001$). The mean in/out-of-phase ratio of the benign nodes was significantly lower than that of the malignant nodes.

Conclusions CSI can differentiate between malignant and benign lymph nodes with a cutoff value of in/out-phase ratio of 0.9. Also, adding the diffusion-ADC map can prefer the same value with a cutoff value of 0.9×10^{-3} cm^2/s. Adding CSI sequence to conventional MRI in examining the nodal status in patients with head and neck primary can enhance diagnostic accuracy of the examination.

Keywords MRI, Lymph node, Chemical shift, Imaging

Background

Cervical lymphadenopathy is classified into: malignant and benign. Malignancy includes primary lesions as lymphoma, multiple myeloma and acute lymphoblastic leukemia [1–3]. Metastatic cervical nodes are more common, and distinction from benign ones is crucial for selection of proper treatment plan [4–6]. Benign etiologies include infectious, autoimmune, lipid storage

*Correspondence:
Lamya Eissa
lamya.eissa@gmail.com
[1] Radiology Department, Alexandria Faculty of Medicine, Alexandria 21131, Egypt

diseases and even medications [6, 7]. Also, recent studies showed that cervical lymphadenopathy could be associated with vaccines, like COVID-19, and they can even mimic malignant nodes in their morphological features [7].

US is the most financially reasonable and accessible in most healthcare providers [8–10] However, it cannot be used accurately in assessing deeper lymph nodes. Color Doppler can increase the diagnostic power by examining nodal vascularity. CT is pioneer in staging and finding primary as well as anatomical localization of nodal level [1, 11–16]. PET/CT adds functional data to already superior anatomical CT details [17–21].

Conventional MRI is highly reliable in evaluation of the cervical nodes. It provides additional information on intra-nodal texture including GAD enhancement and the presence of necrosis or hila [22–24]. Molecular diffusion is visualized via diffusion-weighted imaging (DWI). The signal intensity visible on diffusion is influenced by cell size, density and integrity. This approach is a useful as a supplemental tool for distinguishing malignant from benign nodal tissues as both groups have different intracellular densities, which should reflect as variant ADC values [25–32].

The chemical shift imaging is defined as the variance in the signal intensities produced from inherent variances in the resonant frequencies of precessing fat and water protons [33–35]. Fat molecules have greater shielding of protons if compared to water molecules. Therefore, the protons present in fat molecules precess at a lower frequency than the protons present in water. The variation in frequency between fat and water is known as the "chemical shift effect." This effect is utilized during in-phase (IP) and out-of-phase (OP) imaging in CSI. Chemical shift imaging is basically able to identify microscopic or intracellular fat, and it does not suppress the macroscopic fat [36–39]. In addition, the usage CSI would verify benignity of LNs by confirming the presence of fat in their hila. The problem of both CSI and diffusion is that both benign and malignant categories can reflect overlapping results and both techniques can be affected by artifacts from nearby tissues. The aim of our study was to investigate the role of chemical shift imaging in differentiation between benign and malignant lymph nodes [39].

Patients and methods

(I) *Patients*: This research aimed at patients from the "Oncology," "otorhinolaryngology" and "head and neck surgical wards" with cervical lymphadenopathies, referred to the Radiology department of our Main University Hospitals for MR imaging. The protocol of this *prospective* study was approved by the "Ethics Committee" of our medical institution, and an informed consent was taken from the patients prior to examinations. We aimed to collect patient's in duration from December 2021 to December 2022. *Inclusion criteria* included patients with cervical lymphadenopathy (>5 mm long axis, clinically palpable or routine follow-up of cancer patients), while *exclusion criteria* included (a) claustrophobic patients, (b) patients with metallic foreign bodies, (c) patients with history of radiotherapy and chemotherapy.

All included patients underwent the following: (a) history taking and thorough clinical examination, (b) detailed examination and palpation of the lymph nodes by a well-trained surgeon, (c) ultrasound-guided core or needle biopsy and/or excision biopsy was done for all the patients (according to the patients' provisional diagnosis), and histopathological data were correlated. In some cases, clinical follow-up was satisfactory.

MR images were performed on a 1.5 T system (Achieva 1.5 Tesla, Philips Medical Systems) by using a 16-channel sense neurovascular head and neck coil. All patients underwent DWI MRI and chemical shift imaging examination in addition to conventional MRI. (*I*) *conventional MRI protocol:* MRI protocol was tailored to cover the entire neck. The standard MR neck acquisition parameters were as follows: (a) rapid scout images, (b) multiplanar (axial, coronal and sagittal) T2-weighted, (c) fast spin-echo images (TR, 5000 ms; TE, 102 ms; averages, 2; matrix, 256×256; section thickness, 5.0 mm; and gap, 2.5 mm), (d) axial T1-weighted images (TR, 675 ms; TE, 8 ms; averages, 2; section thickness, 5.0 mm; gap, 2.5 mm; matrix, 256×256), (e) standard T1- and T2-weighted imaging was followed by DWI and in and out phases, and (f) characterization of the LNs by conventional MRI depends on the nodal morphology. According to Flavio Barchetti et al. [40], the lymph node was considered pathological if it fulfilled one or more of the following *criteria* (*on T2 images*) [41]: (a) *oval shape* with short axis more than 10 mm, (b) *round* shape with diameter more than 8 mm, (c) internal necrosis regardless the shape and size, (d) heterogeneous intensity or indistinct borders. Additional signs of malignancy include: T2 heterogeneous signal, heterogeneous GAD enhancement (if GAD was given) and irregular margins (Figs. 1, 2, 3, 4, 5, 6, 7 and 8).

(II) *DWI MRI*: DWI was performed by using a single-shot spin-echo EPI sequence with the following parameters (single-shot turbo spin-echo (SS-TSE)-DWI sequence was used): axial plane 4-mm section thickness, FOV of 240 mm and *b*-values of 0 and 1000 s/mm^2. ADC maps were generated from the DWIs where ROIs were placed on the DWIs and were copied to the corresponding ADC map, and then, ADC values were calculated using the workstation software. ROIs were placed upon

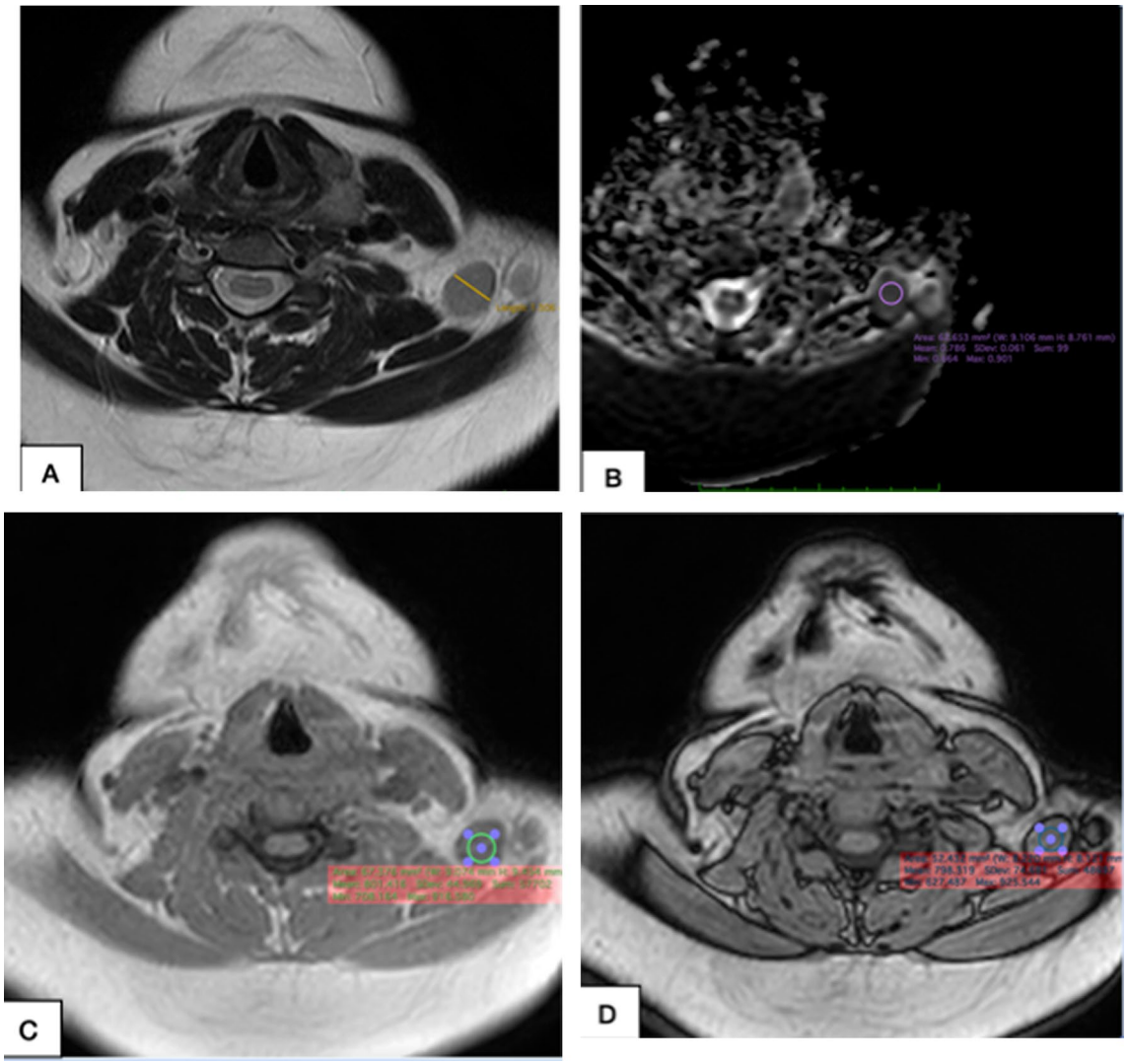

Fig. 1 ROC curve for ADC value to discriminate malignant ($n=22$) from benign ($n=9$)

solid portions of the lesion avoiding necrotic areas. Three ADC values were calculated, and the mean ADC was the value used in statistical analysis. The mean ADC values in the benign and malignant groups were compared using Mann–Whitney test and others (detailed below in statistical analysis). We used qualitative evaluation of the signal intensity in b-1000 images and described the lesion as hypointense (not restricted) or hyperintense (restricted) subjectively.

(III) *Chemical shift imaging*: Dual chemical shift sequences for OP and IP images with breath-holding were obtained at TR/TE_110/2.3 ms (OP images) and TR/TE_110/4.7 ms (IP images). The flip angle was 90°. The duration of these sequences was 32 s, yielding seven slices. All images were then sent to a PACS workstation, and the lymph nodes noted on the T1 and T2 sequences were identified on the in-phase/opposed-phase (IP/OP) sequences. Three measurements of the signal intensity were made, and the average recorded and IP/OP ratios were calculated by measuring signal intensities in every image (via adequate ROI like ADC) and dividing the values in in phase by that in out-of-phase images.

(IV) *Statistical analysis of the data*: Data were fed to the computer and analyzed using IBM SPSS software package version 20.0. (Armonk, NY: IBM Corp). Qualitative data were described using number and percent. The Shapiro–Wilk test was used to verify the normality of distribution. Quantitative data were described using range (minimum and maximum), mean, standard deviation, median and interquartile range (IQR).

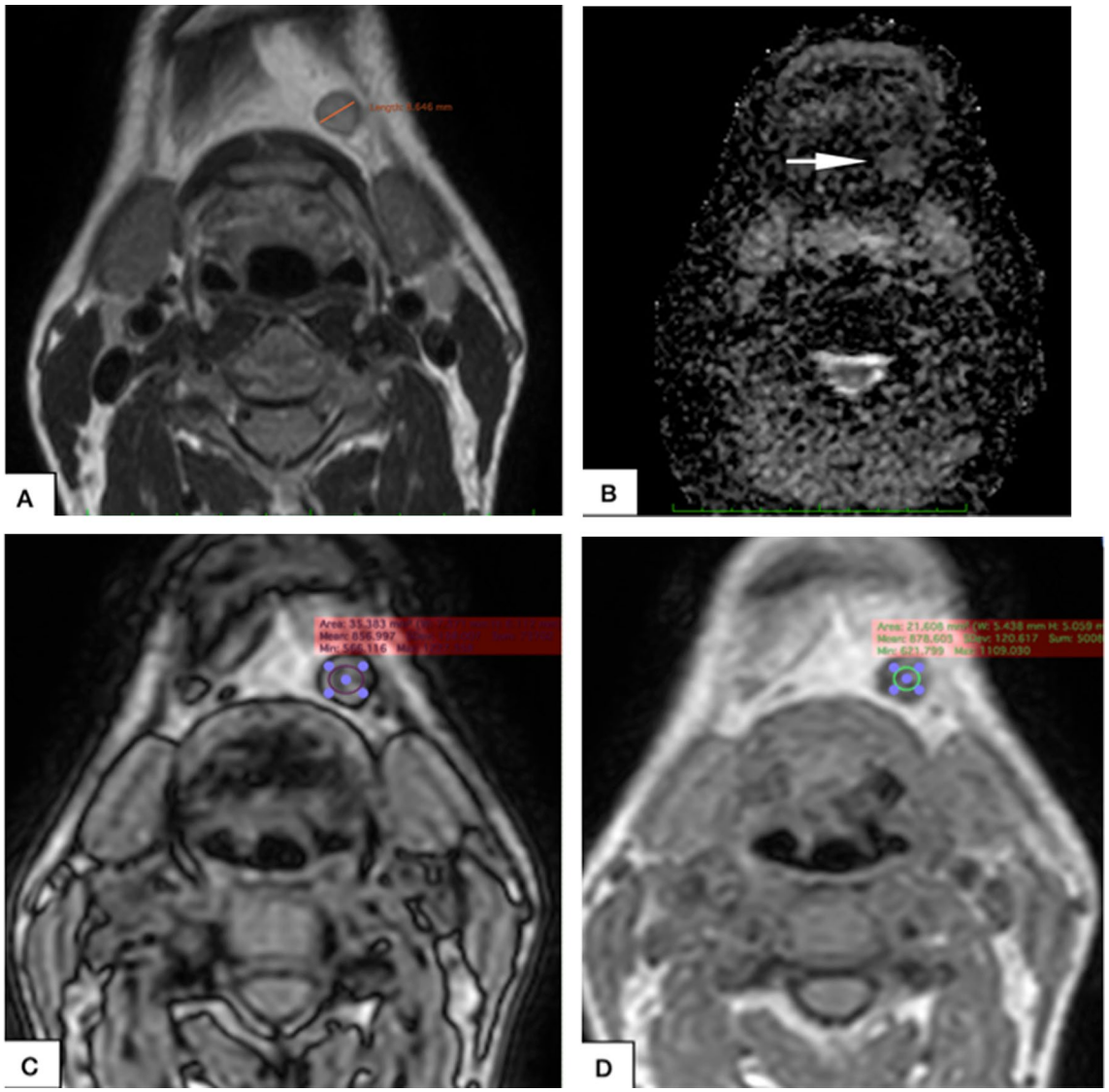

Fig. 2 Female patient 32 years old presenting with papillary thyroid cancer and left level V cervical lymphadenopathy. Axial T2 image **A** shows homogenous signal of the node seen rounded measuring 13 mm in short axis. The LN shows restricted diffusion **B** with low ADC value (0.72) in ADC map reflecting malignant nature of the lesion. The LN showed loss of signal drop on CSI **C**, **D** with in/out-of-phase ratio of 0.997. By histopathology, the lesion proved to be metastatic

Significance of the obtained results was judged at the 5% level. *The used tests were*: (1) *chi-square* test for categorical variables, to compare between different groups, (2) *Fisher's exact or Monte Carlo correction* for chi-square when more than 20% of the cells have expected count less than 5, (3) *Student's t test* for normally distributed quantitative variables, to compare between two studied groups, (4) *Mann–Whitney test* for abnormally distributed quantitative variables, to compare between two studied groups.

Results

This study was conducted on 31 patients presenting with cervical lymphadenopathy. Patients included 17 males and 15 females with ages averaging between 28 and 70 years. A single inflammatory node was pathologically proven of tuberculous origin and was studied by imaging; yet not included in the statistics. We studied metastatic cervical lymph nodes of different primaries including papillary thyroid cancer, lymphoma, and squamous cell carcinomas of different origins as well

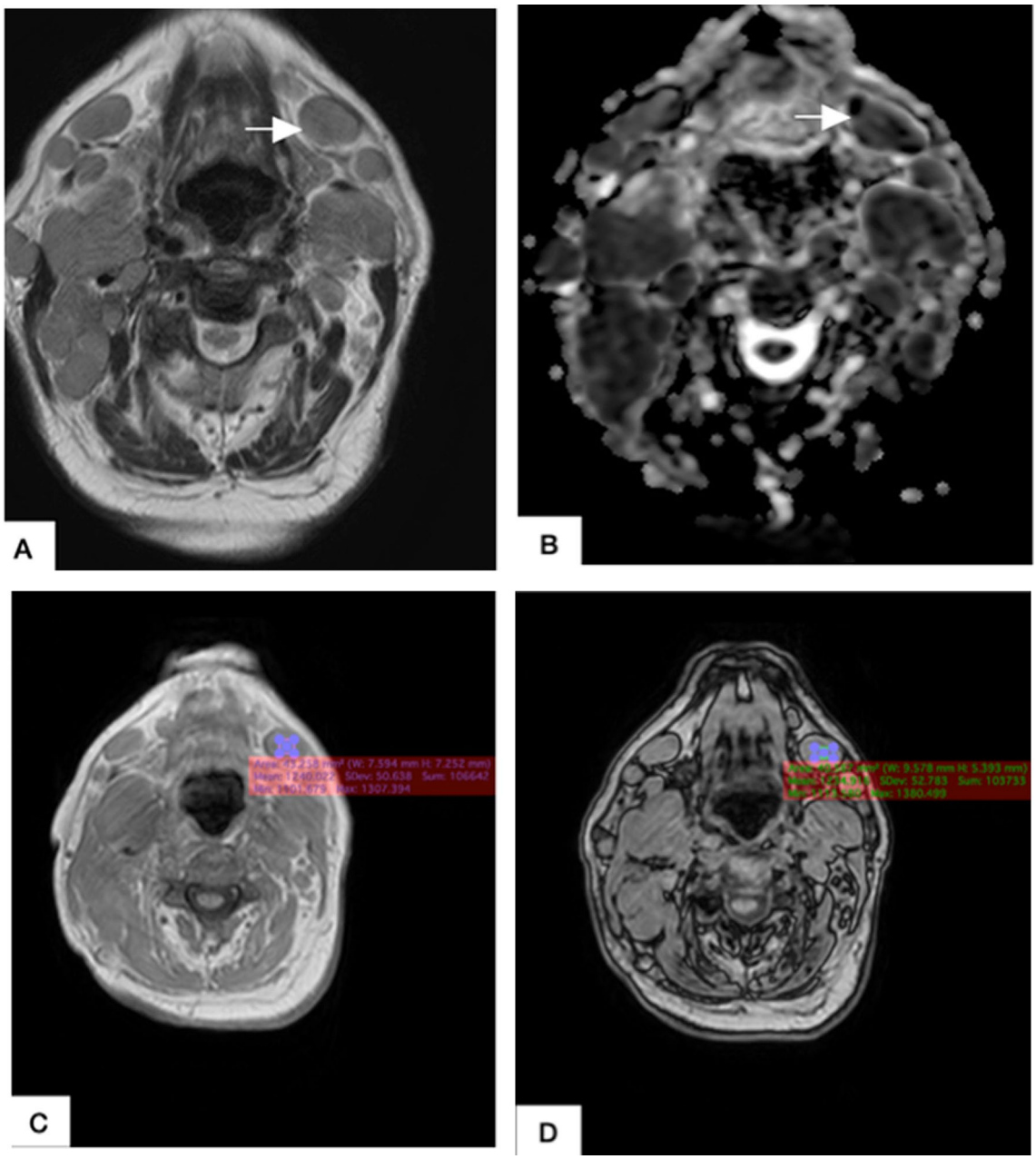

Fig. 3 Male patient 35 years old presenting with squamous cell carcinoma of the tongue and left level IA lymphadenopathy. Axial T2 image **A** shows homogenous signal of the node seen rounded measuring 8 mm in short axis. The ADC map **B** shows restricted diffusion of the submental LN (white arrow) with ADC value (0.7) in ADC map. The LN showed loss of signal drop on CSI **C**, **D** with in/out-of-phase ratio of 0.974. Core biopsy from the LN proved to be metastatic

as mucoepidermoid carcinoma. Table 1 provides distribution of different pathologies. Twenty-one patients received GAD injection; remaining 10 patients did not because of bad renal functions.

Pathological diagnosis of the LNs was obtained via ultrasound-guided biopsy or following excisional biopsy after neck dissection. According to the histopathology; twenty-two LNs were found to be malignant and nine LNs were benign. (All of our cases underwent cytology by excision except a case with known cancer and small nodes suggested by conventional MRI and more suggested by CSI and DWI as being only reactive by US-FNA). Follow-up was done to patients who presented with reactive nodes and no primary.

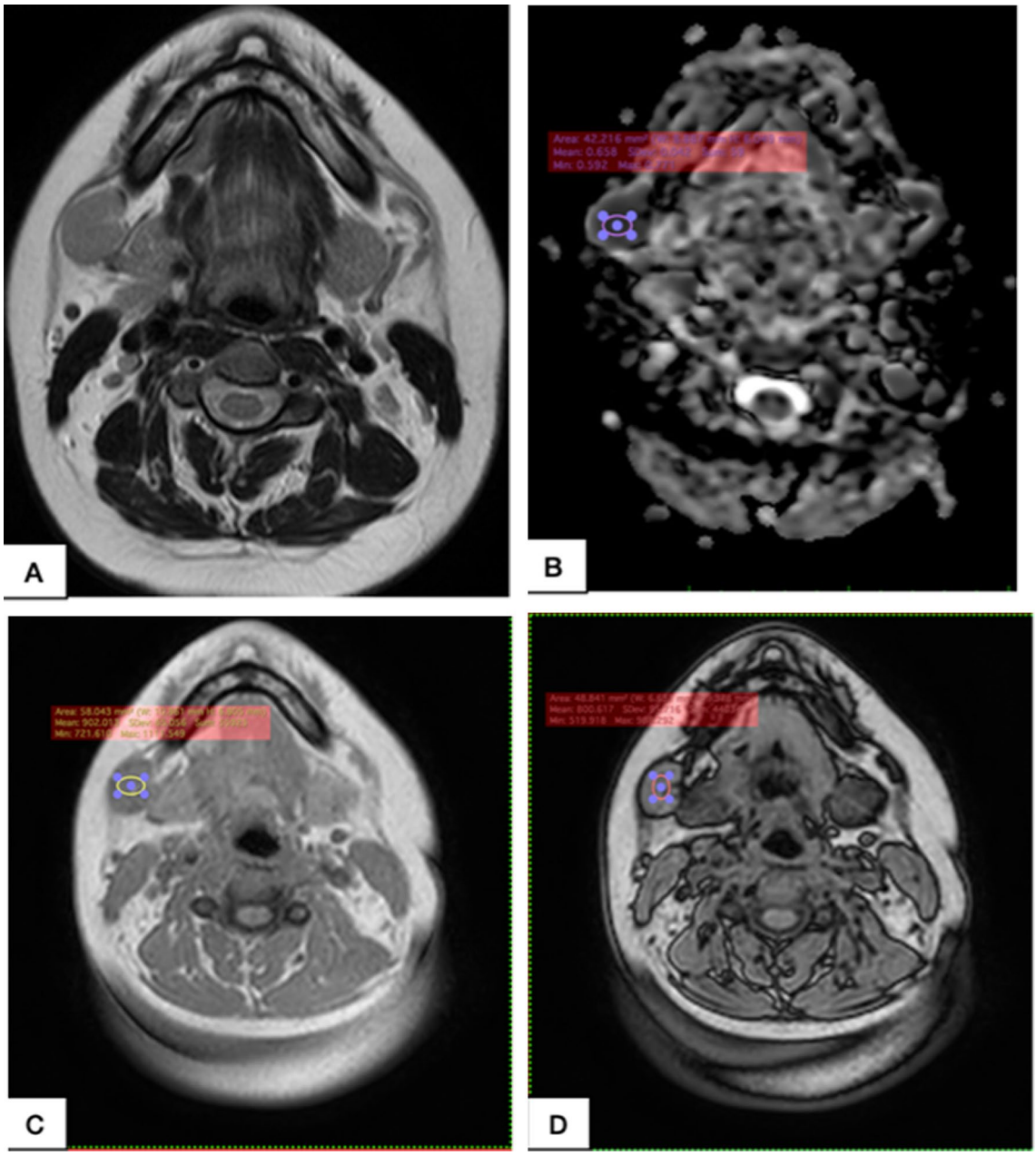

Fig. 4 Male patient 65 years old presenting with lymphoma and multiple cervical lymphadenopathy. The LN studied was left level IB. Axial T2 image **A** shows homogenous signal of the node (white arrow) seen rounded measuring 13 mm in short axis. The ADC map **B** shows restricted diffusion (white arrow) of the node with ADC value (0.6) in ADC map. The LN showed loss of signal drop on CSI **C**, **D** with in/out-of-phase ratio of 0.9. Core biopsy from the LN proved to be non-Hodgkin lymphoma

Conventional MRI was made, and T2 morphology was studied according to Flavio Barchetti et al. [40] criteria. The sensitivity of conventional MRI according to the previously mentioned criteria is 90.91%, while it has a relatively low specificity for metastatic lymph node reaching 66.67%, and the PPV was 86.96%, and the NPV was 75%, while the accuracy was 83.87%. These are summarized in Tables 2 and 3.

Table 3 shows the mean ADC values of the malignant and benign lymph nodes. The mean ADC values of the benign and malignant LNs were 1.06 ± 0.25 and 0.85 ± 0.24, respectively. A statistically significant difference was found between the two groups ($p = 0.041$). The mean ADC values of the malignant LNs were significantly lower ($p = 0.001$) than those of the benign LNs. An ADC value of 0.9×10^{-3} mm^2/s was concluded to be the

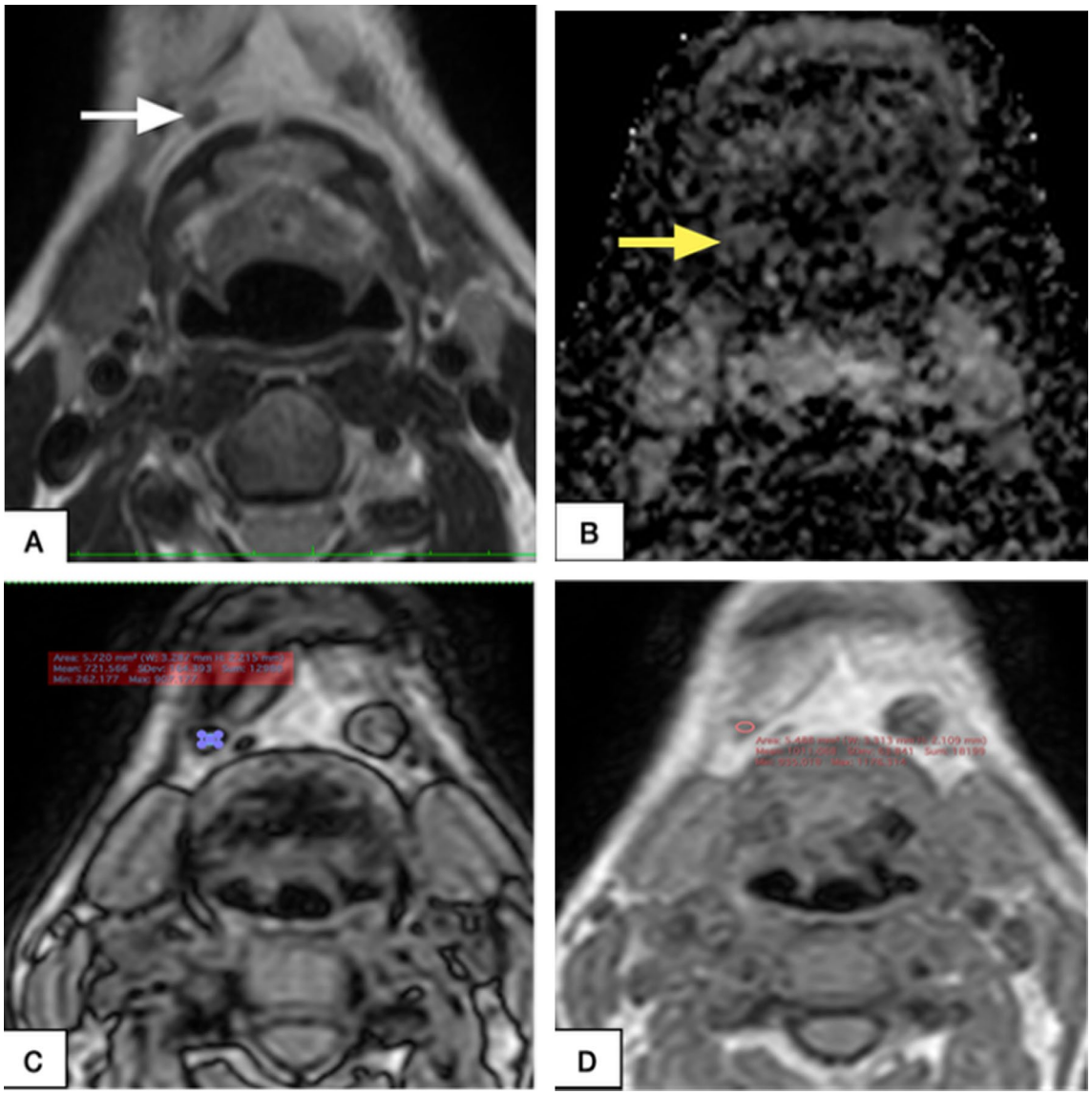

Fig. 5 Female patient 32 years old presenting with papillary thyroid cancer and right Level II cervical lymphadenopathy. Axial T2 image **A** shows homogenous signal of the node seen oval measuring 18 mm in short axis. The LN shows restricted diffusion **B** with low ADC value (0.6) in ADC map reflecting malignant nature of the lesion. The LN showed signal drop on CSI **C**, **D** with in/out-of-phase ratio of 0.88. By excisional biopsy, the LN was proved to be reactive

best cutoff value for differentiating benign from malignant LNs. It showed a diagnostic accuracy of 72.77% sensitivity and 88.7% specificity shown in Table 4.

Table 5 shows the mean values (in/out-of-phase ratio) of the benign and malignant lymph nodes. The mean values of the benign and malignant LNs were 0.75 ± 0.16 and 0.96 ± 0.06, respectively. A statistically significant difference was found between the two groups (p, 0.001). The mean in/out-of-phase ratio of the benign LNs was significantly lower than that of the malignant LNs. A cutoff value of approximately 0.9 was concluded to be the best cutoff value for differentiating benign from malignant LNs. It showed a diagnostic ability of 95.45% sensitivity and 88.89% specificity, shown in Table 5.

Discussion

Head and neck malignancies represent about 4% of the malignancies of the body [41]. This study aims to differentiate between nodes without the need of unnecessary biopsies and without the need of intravenous contrast, thus avoiding their complications. Gor et al. [42] stated that the size of the lymph node is not a reliable sole indicator with false-positive value 15% and false-negative value 20%. Many malignant nodes showed normal size,

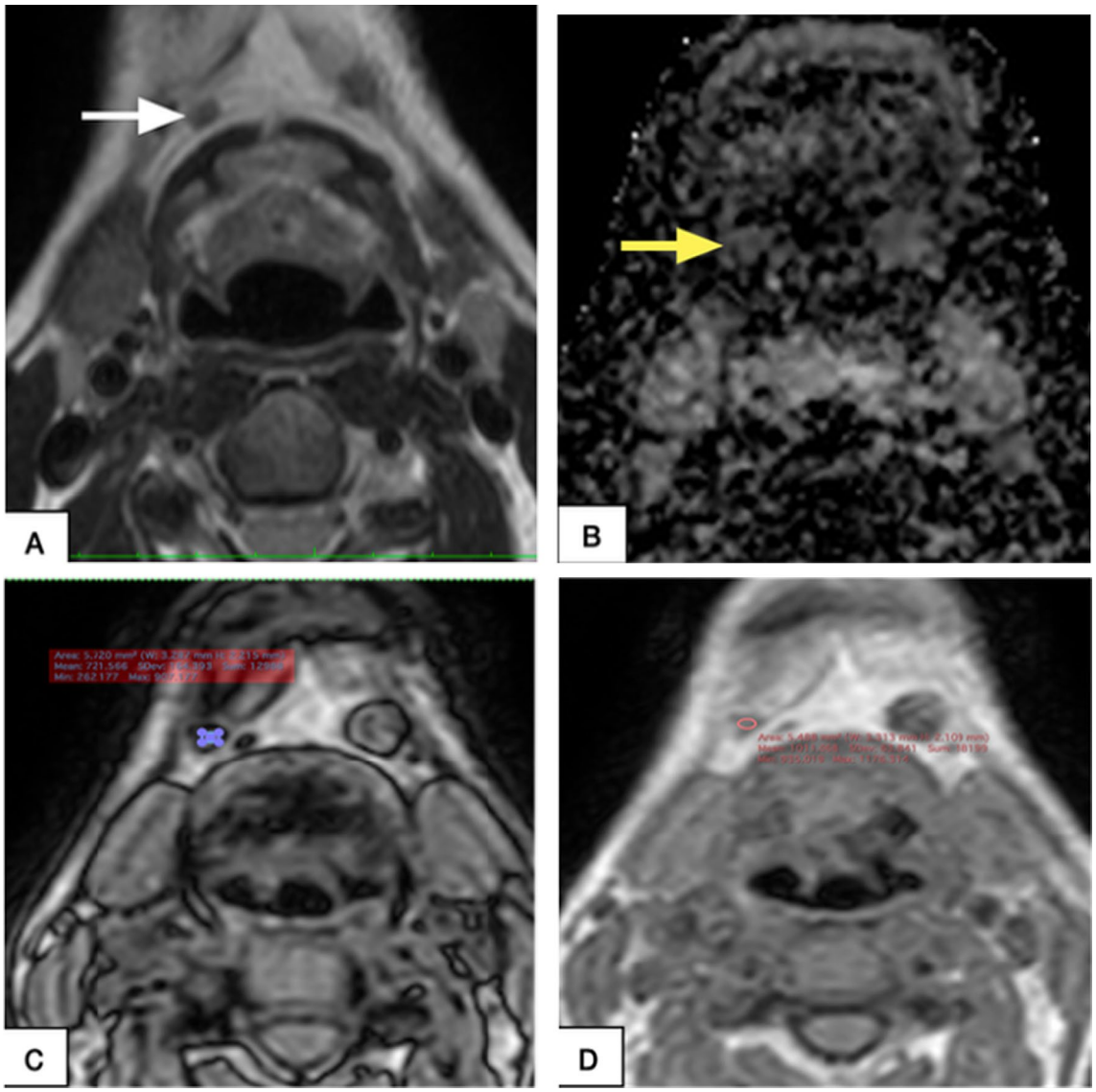

Fig. 6 Male patient 35 years old presenting with squamous cell carcinoma of the tongue and right level Ia lymphadenopathy. Axial T2 image **A** shows homogenous signal of the node seen rounded measuring 3 mm in short axis. The ADC map **B** shows restricted diffusion of the submental LN (yellow arrow) with ADC value (0.7) in ADC map. The LN showed signal drop on CSI **C**, **D** with in/out-of-phase ratio of 0.71. Biopsy from the LN proved to be metastatic

while on the contrary enlarged lymph nodes may be of benign cause. Gor et al. [42] also stated that it is not specific to depend on the lymph node's shape; benign nodes are usually kidney shaped, while malignant nodes are usually rounded (Tables 6 and 7).

Barchetti et al. [40], in their study of patients with squamous cell carcinomas in the head neck, stated that a combination of morphological criteria may suggest diagnosis. He included the size of the node and concluded that central and eccentric necrosis is a strong indicator of malignancy disregarding the size of the node. According to these criteria, we found three false-positive results and two false-negative results. The reason of these falsies was due to depending on the size of the node as an indicator for malignancy. Necrosis within the node as well as heterogeneous T2 signal was always coupled with malignant nodes; all the benign nodes showed homogenous signal intensity, except the excluded one of tuberculous origin where diagnosis is readily made.

In this study, there was a significant difference in the ADC values between benign and malignant lymph nodes matching the findings with prior studies; malignant lymph nodes had a relatively lower ADC values than that of malignant nodes yet there was an overlap between

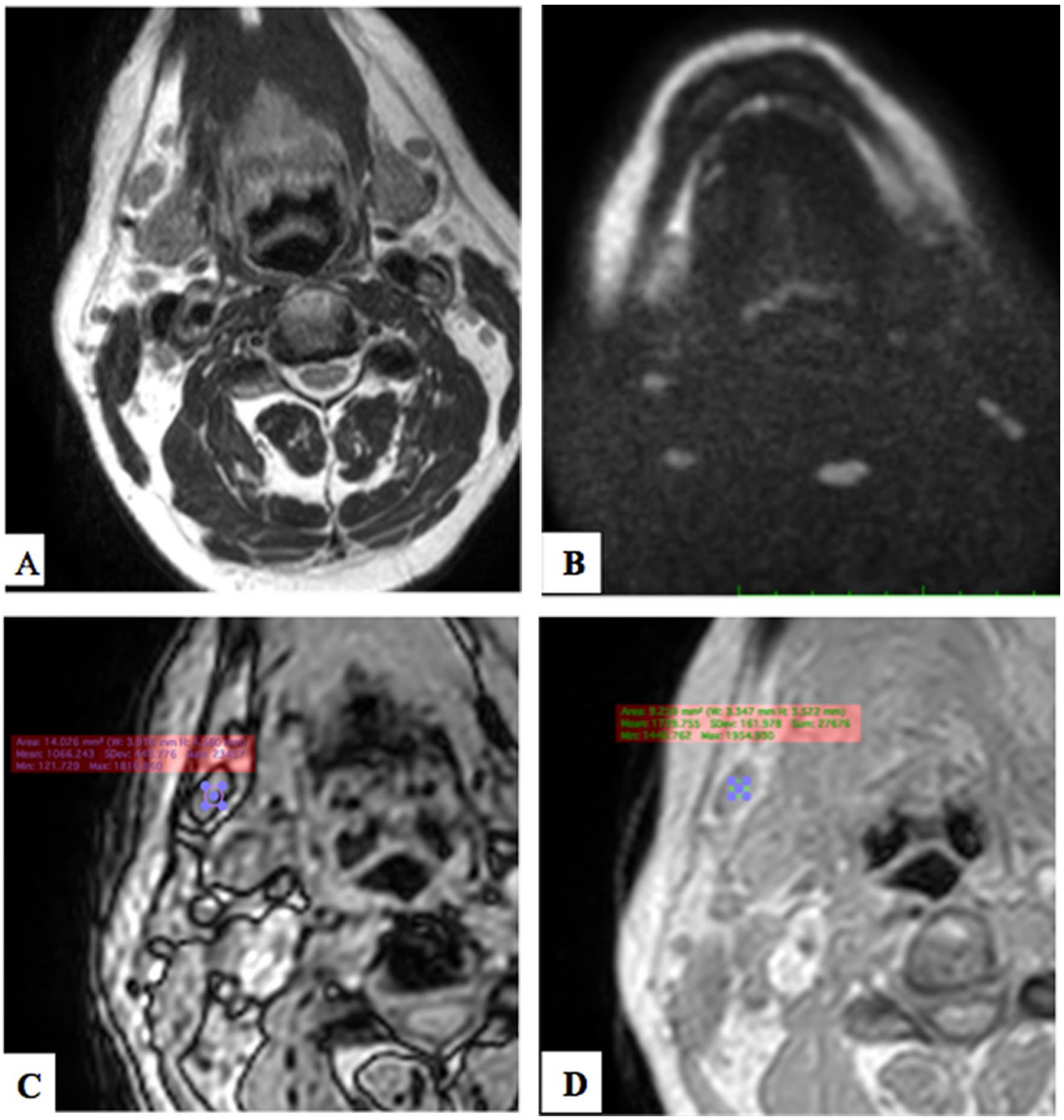

Fig. 7 Male patient 56 years old presenting with nasopharyngeal carcinoma and right level Ib LN. Axial T2 image **A** shows homogenous oval shaped LN measuring 7 m in short axis. The LN is hypointense on B1000; **B** shows no restricted diffusion with ADC value (1.12) in ADC map. The LN showed signal drop on CSI **C**, **D** with in/out-of-phase ratio of 0.617. Cytological assessment and follow-up revealed its benignity

them. We concluded that the best cutoff ADC value is 0.9×10^{-3} mm^2/s. The mean ADC of metastatic was much lower than the mean of benign LNs with specificity 87.5% and sensitivity 72.7%. We studied 7 patients with lymphoma as primary; they all showed restricted diffusion with lower ADC values than most of the metastatic nodes; they ranged from 0.6×10^{-3} to 0.9×10^{-3} mm^2/s. Survov et al. [43] also agreed with this finding; he proposed that lymphomatous nodes have lower ADC values reaching 0.7×10^{-3} mm^2/s. There was one false-positive result in a case of lymphoid hyperplasia. This may be due to the proliferation of lymphocytes compacting the lymph node thus slightly hindering the motion of molecules to some extent, thus resulting in restricted movement and low ADC value.

There were six false-negative results in our study: Three of them were papillary thyroid carcinoma, two were metastatic squamous cell carcinoma and one case of metastatic nasopharyngeal carcinoma. The high ADC values of those nodes may be due to the necrotic nature of the nodes. Singh et al. [43] concluded that a cutoff ADC value of 1.01×10^{-3} mm^2/s is optimum to differentiate between

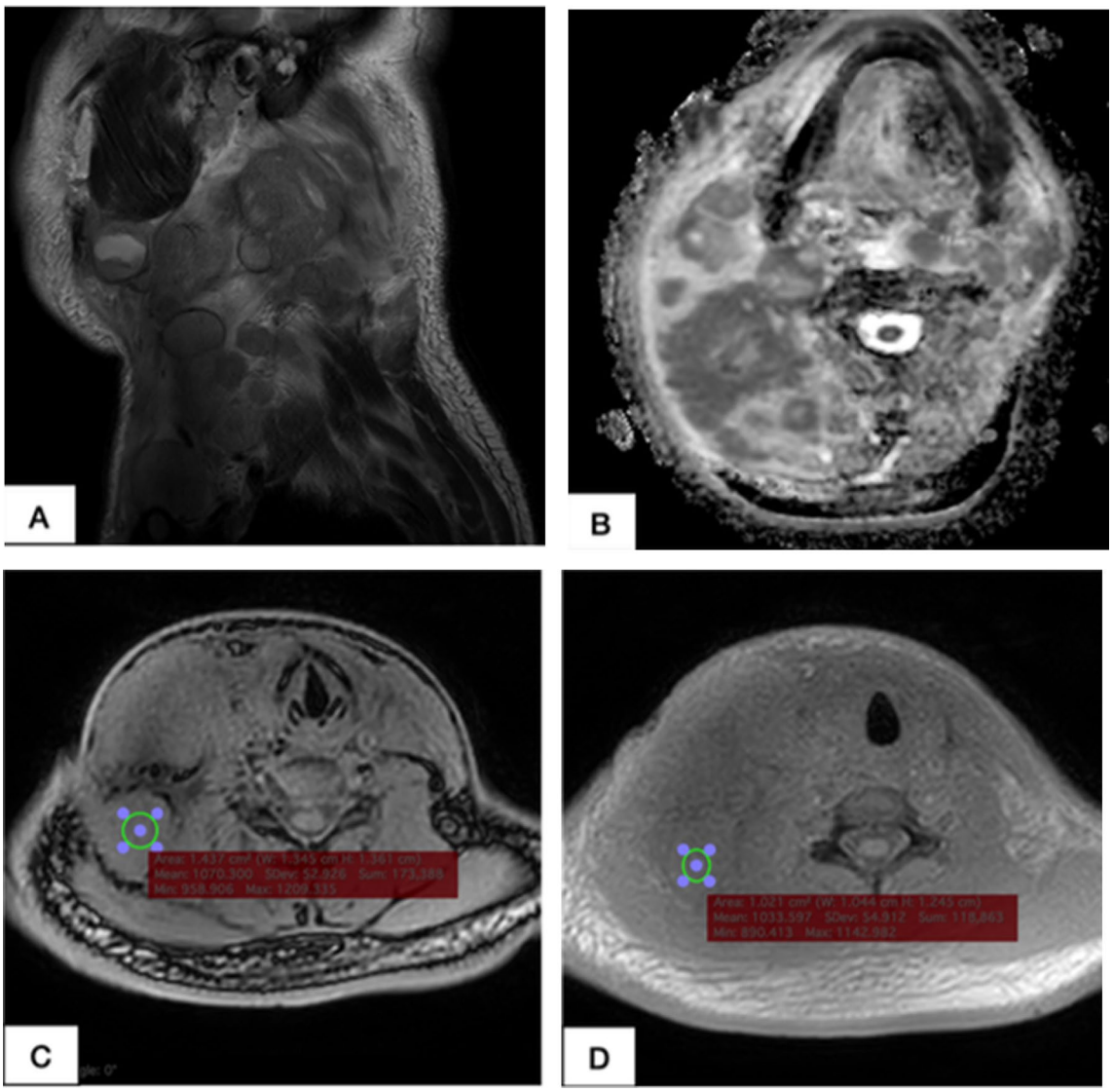

Fig. 8 Male patient 48 years old presenting with cervical lymphadenopathy. The LN studied was at right level V. Sagittal T2 image **A** shows heterogeneous signal of the node with internal necrosis and amalgamated borders; it is seen rounded measuring 27 mm in short axis. The ADC map **B** shows restricted diffusion of the LN with ADC value (0.9) in ADC map. The LN showed loss of signal drop on CSI **C**, **D** with in/out-of-phase ratio of 0.92. Core biopsy proved the LN to be tuberculous lymphadenopathy

benign and malignant cervical lymph nodes with sensitivity 97% and specificity 91.1%. Chong et al. [44] proposed an ADC cutoff value of 0.965×10^{-3} mm^2/s, yet his study was concerned only with the study of squamous cell carcinomas of the head and neck.

In our study, sinus fat within the node was considered present if there was a drop of signal between the in and out of phases, while the absence of signal drop denotes malignant nodes. Zhang et al. [45] studied the role of CSI in characterizing the nodal status of the lymph nodes in rectal nodes. The study was based on the concept of the signal drop of the fatty hilum of benign nodes, while metastatic nodes are invaded by metastatic tissue obliterating the sinus fat leading to the loss of signal drop [45].

The principle of CSI is based on the fact that precession frequencies of hydrogen protons in water and fat molecules are variable. This means that on excitation they will be in phase and out of phase repeatedly. When they are out of phase, the fat and water will cancel each other. Therefore, there will be loss of signal in out-phase sequences [33, 34, 46]. As established in vertebral body malignancy, Mittal et al. [46] used CSI to differentiate between benign and malignant vertebral collapse with

Table 1 Distribution of the studied cases according to the presenting primary ($n=31$)

Type of malignancy	No	%
No tumor	2	6.5
Submandibular squamous cell carcinoma	1	3.2
Submandibular mucoepidermoid	1	3.2
Skin squamous cell carcinoma	2	6.5
Papillary thyroid carcinoma	9	29.0
Papillary squamous cell carcinoma	1	3.2
Nasopharyngeal carcinoma	3	9.7
Mucoepidermoid carcinoma	1	3.2
Lymphoma	7	22.6
Lymphoid hyperplasia	1	3.2
Cancer tongue	3	9.7

cutoff value 0.95. We adapted the same approach, a ratio between the "in-phase" and "out-of-phase" images.

The in/out ratio cutoff value suggested by our study was 0.9; below it was considered benign while above this value was considered malignant. The sensitivity of the CSI study was 95.45%, while the specificity was 88.8%. The false positive was a case of lymphoid hyperplasia with in/out-phase ratio 0.96. This may be due to the presence of nodal reactive change, which compresses the fatty hilum making it imperceptible by the ROI, thus making our readings inaccurate. The false negative was a case of squamous cell carcinoma of the tongue with metastatic submental nodes. The short axis of the node was less than 3 mm, and thus, inaccurate measurement of the

Table 2 Comparison between benign and malignant according to different parameters on conventional T2

ADC value	Total ($n=31$)	ACC to pathology		*t*	*p*
		Benign ($n=9$)	Malignant ($n=22$)		
Min–Max	0.40–1.40	0.50–1.40	0.40–1.40	2.144*	0.041*
Mean ± SD	0.91 ± 0.26	1.06 ± 0.25	0.85 ± 0.24		
Median (IQR)	0.90 (0.70–1.08)	1.07 (1.03–1.20)	0.85 (0.70–1.04)		

IQR: Inter-quartile range; SD: Standard deviation; *t*: Student's *t* test; and *p*: *p* value for comparing between benign and malignant

*Statistically significant at $p \leq 0.05$

Table 3 Agreement (sensitivity, specificity and accuracy) for T2 sequence

	AUC	*p*	95% CI	Cutoff[#]	Sensitivity	Specificity	PPV	NPV
ADC value	0.775*	0.028*	0.549–0.961	≤ 0.9[#]	72.7	88.7	93.7	53.3

AUC: Area under a curve; *p* value: probability value; CI: confidence intervals; NPV: negative predictive value; and PPV: positive predictive value

[*] Statistically significant at $p \leq 0.05$

[#] Cutoff was choose according to Youden index

Table 4 Comparison between benign and malignant according to ADC value

	Total ($n=31$)	ACC to pathology		Test of Sig	*p*
		Benign ($n=9$)	Malignant ($n=22$)		
In phase					
Min–Max	249.0–2054.0	683.0–1729.0	249.0–2054.0	$t=1.483$	0.149
Mean ± SD	1222.9 ± 412.2	1054.6 ± 307.2	1291.7 ± 435.5		
Median (IQR)	1196.0 (915.5–1473.0)	965.0 (868.0–1196.0)	1280.5 (996.0–1590.0)		
Out of phase					
Min–Max	236.0–2017.0	303.0–1183.0	236.0–2017.0	$t=2.944$*	0.006*
Mean ± SD	1116.8 ± 447.6	786.7 ± 247.5	1251.9 ± 443.9		
Median (IQR)	1125.0 (799.0–1350.5)	780.0 (697.0–822.0)	1267.5 (867.0–1587.0)		
Ratio in/out					
Min–Max	0.44–1.0	0.44–0.97	0.71–1.0	U = 12.0*	< 0.001*
Mean ± SD	0.90 ± 0.14	0.75 ± 0.16	0.96 ± 0.06		
Median (IQR)	0.96 (0.86–0.99)	0.80 (0.68–0.83)	0.98 (0.96–0.99)		

IQR: Inter-quartile range; SD: standard deviation; *t*: Student's *t* test; U: Mann–Whitney test; and *p*: *p* value for comparing between benign and malignant

*Statistically significant at $p \leq 0.05$

Table 5 Validity (AUC, sensitivity, specificity) for ADC value to discriminate malignant ($n=22$) from benign ($n=9$)

	AUC	*p*	95% CI	Cutoff[#]	Sensitivity	Specificity	PPV	NPV
Ratio in/out	0.939*	< 0.001*	0.849–1.030	> 0.9[#]	95.45	88.89	95.5	88.9

AUC: Area under a curve; *p* value: probability value; CI: confidence intervals; NPV: negative predictive value; and PPV: positive predictive value

*Statistically significant at $p \leq 0.05$

[#] Cutoff was choose according to Youden index

Table 6 Comparison between benign and malignant according to chemical shift ratio (in/out of phase) value

	Total ($n=31$)	ACC to pathology		Test of sig	*p*
		Benign ($n=9$)	Malignant ($n=22$)		
In phase					
Min–Max	249.0–2054.0	683.0–1729.0	249.0–2054.0	$t=1.483$	0.149
Mean ± SD	1222.9 ± 412.2	1054.6 ± 307.2	1291.7 ± 435.5		
Median (IQR)	1196.0 (915.5–1473.0)	965.0 (868.0–196.0)	1280.5 (996.0–1590.0)		
Out of phase					
Min–Max	236.0–2017.0	303.0–1183.0	236.0–2017.0	$t=2.944$*	0.006*
Mean ± SD	1116.8 ± 447.6	786.7 ± 247.5	1251.9 ± 443.9		
Median (IQR)	1125.0 (799.0–1350.5)	780.0 (697.0–822.0)	1267.5 (867.0–1587.0)		
Ratio in/out					
Min–Max	0.44–1.0	0.44–0.97	0.71–1.0	U = 12.0*	< 0.001*
Mean ± SD	0.90 ± 0.14	0.75 ± 0.16	0.96 ± 0.06		
Median (IQR)	0.96 (0.86–0.99)	0.80 (0.68–0.83)	0.98 (0.96–0.99)		

IQR: Inter-quartile range; SD: standard deviation; *t*: Student's *t* test; U: Mann–Whitney test; and *p*: *p* value for comparing between benign and malignant

*Statistically significant at $p \leq 0.05$

Table 7 Validity (AUC, sensitivity, specificity) for ratio in/out to discriminate malignant ($n=22$) from benign ($n=9$)

	AUC	*p*	95% CI	Cutoff[#]	Sensitivity	Specificity	PPV	NPV
Ratio in/out	0.939*	< 0.001*	0.849–1.030	> 0.9[#]	95.45	88.89	95.5	88.9

AUC: Area under a curve; *p* value: probability value; *CI*: confidence intervals; *NPV*: negative predictive value; and *PPV*: positive predictive value

*Statistically significant at $p \leq 0.05$

[#] Cutoff was choose according to Youden index

ROI due to the spatial resolution led to the false-negative measurement.

Our study included one inflammatory case (which was not included in the statistical analysis); it was a case of cervical tuberculous lymphadenitis, which was already easily diagnosed by clinical and conventional criteria. Both diffusion and CSI failed to differentiate between inflammatory and malignant changes in this case. Both showed findings supporting the findings of malignancy: a low ADC value of $O.9\times10^{-3}$ mm^2/s and loss of signal drop on CSI with in/out ratio more than 0.9. The morphological features on conventional imaging showed internal necrosis and amalgamated irregular margins.

The CSI was found to be more sensitive and specific in tissue characterization of the cervical lymph node than diffusion-weighted images and conventional MRI. The false-positive and false-negative results of the ADC value with cutoff value 0.9×10^{-3} mm^2/s were corrected by the in/out-phase ratio with cutoff value 0.9. Only one patient—a case of lymphoid hyperplasia—where both CSI and diffusion failed to characterize it and suggested it to be malignant although histopathological assessment revealed the absence of malignancy. However, diffusion was able to characterize smaller LN which measured 3 mm in short axis yet CSI failed to identify it accurately.

We agreed with Survov et al. [43] that ADC values play a limited role in distinguishing between malignant and benign lesions. Primary assessment of cervical lymphadenopathy by either diffusion or chemical shift imaging alone is not advised to avoid fallacies caused by reactive inflammatory nodes and lymphoid hyperplasia. Thus, combining both CSI and diffusion provides diagnostic

accuracy or even the usage of CSI as a sole indicator for characterization of metastatic LNs yields good results thus reducing unnecessary biopsies and intravenous contrast. Nevertheless, our study had a few *limitations*. First, the number of the lymph nodes studied was relatively small and this is limited because of workflow potentially hindered by cumulative small time on machine added by the sequence with its economic burden. Second, selection of optimal sites for localization of ROIs would affect the consistent acquisition of reliable ADC and CSI values.

Conclusions

We made some conclusions from our study: CSI can differentiate between malignant and benign lymph nodes with a cutoff value of in/out-phase ratio of 0.9. Also, adding the diffusion-ADC map can prefer the same value with a cutoff value of 0.9×10^{-3} cm^2/s. Adding CSI sequence to conventional MRI in examining the nodal status in patients with head and neck primary can enhance diagnostic accuracy of the examination.

Abbreviations

MRI	Magnetic resonance imaging
CT	Computed tomography
TR	Time of repetition
TE	Time of echo
GAD	Gadolinium
FOV	Field of view
ADC	Apparent diffusion coefficient
IP	In phase
OP	Out of phase
CSI	Chemical shift imaging
LN	Lymph node
US	Ultrasound
DWI	Diffusion-weighted imaging
GAD	Gadolinium

Acknowledgements

Not applicable.

Author contributions

MM provided the cases and final diagnoses, with detailed description of results. LE gave the idea, wrote the section of introduction and provided the whole references for introduction and discussion with making of figure legends. "All authors read and approved the final manuscript." RD made the whole final supervision on conducted research and on the written consent.

Funding

This study had no funding from any resource.

Availability of data and materials

The datasets used and/or analyzed during the current study are available from the corresponding author on reasonable request.

Declarations

Ethics approval and consent to participate

All procedures followed were in accordance with the ethical standards of the responsible committee on human experimentation (Institutional Review Board (IRB) of Alexandria General Hospital on 14 February 2022) and with the Helsinki Declaration of 1964 and later versions. Committee's reference number is unavailable (NOT applicable). No consent was obtained from the patients since it was a retrospective study.

Consent for publication

All patients included in this research gave written informed consent to publish the data contained within this study.

Competing interests

The authors declare that they have no competing interests.

Received: 2 May 2023 Accepted: 19 August 2023
Published online: 25 September 2023

References

1. Gaddey HL, Riegel AM (2016) Unexplained lymphadenopathy: evaluation and differential diagnosis. Am Fam Physician 94(11):896–903
2. Liao LJ, Lo WC, Hsu WL, Wang CT, Lai MS (2012) Detection of cervical lymph node metastasis in head and neck cancer patients with clinically N0 neck-a meta-analysis comparing different imaging modalities. BMC Cancer 12:236
3. Kawada K, Taketo MM (2011) Significance and mechanism of lymph node metastasis in cancer progression. Cancer Res 71:1214–1218
4. Elmore SA (2006) Histopathology of the lymph nodes. Toxicol Pathol 34(5):425–454
5. Lang S, Kansy B (2014). Cervical lymph node diseases in children. GMS Curr Top Otorhinolaryngology Head Neck Surg 13
6. Sambandan T, ChristefiMapel R (2011) Review of cervical lymphadenopathy. JIADS 2(1):31–33
7. Abou-Foul AK, Ross E, Abou-Foul M, George AP (2021) Cervical lymphadenopathy following coronavirus disease 2019 vaccine: clinical characteristics and implications for head and neck cancer services. J Laryngol Otol 135(11):1025–1030
8. Shah JP, Montero PH (2018) New AJCC/UICC staging system for head and neck, and thyroid cancer. Revista Médica Clínica Las Condes 29(4):397–404
9. Eisenmenger LB, Wiggins RH (2015) Imaging of head and neck lymph nodes. Radiol Clin North Am 53(1):115–132
10. Bayon R, McClintick S (2013) Cervical node metastases from squamous cell carcinomas, patterns of. In: Kountakis SE (ed) Encyclopedia of otolaryngology, head and neck surgery. Springer, Berlin
11. Misra D, Panjwani S (2016) Rai S (2016) Diagnostic efficacy of color Doppler ultrasound in evaluation of cervical lymphadenopathy. Dent Res J (Isfahan) 13(3):217–24
12. Fish SA, Langer JE, Mandel SJ (2008) Sonographic imaging of thyroid nodules and cervical lymph nodes. Endocrinol Metab Clin North Am 37(2):401–417
13. Ahuj A, Ying M, Ho SY, Antonio G, Lee YP, King AD et al (2008) Ultrasound of malignant cervical lymph nodes. Cancer Imaging 8(1):48–56
14. Zhao Y, Liao X, Wang Y, Lan W, Ren J, Yang N et al (2022) Level Ib CTV delineation in nasopharyngeal carcinoma based on lymph node distribution and topographic anatomy. Radiother Oncol 172:10–17. https://doi.org/10.1016/j.radonc.2022.04.026
15. Pakkanen AL, Marttila E, Apajalahti S, Snäll J, Wilkman T (2022) Reliability of the pre-operative imaging to assess neck nodal involvement in oral cancer patients, a single-center study. Med Oral Patol Oral Cir Bucal 27(2):e191–e197
16. Robbins KT (1991) Standardizing neck dissection terminology: official report of the academy's committee for head and neck surgery and oncology. Arch Otolaryngol Head Neck Surg 117:601–605
17. Yang L, Luo D, Li L (2016) Differentiation of malignant cervical lymphadenopathy by dual-energy CT: a preliminary analysis. Sci Rep 6:31020
18. Eissa LA, Mehanna AM (2020) Imaging of metastatic cervical nodes: is CT helpful in differentiation of squamous cell carcinoma (SCC) from non-SCC groups? Egypt J Otolaryngol 36:45
19. Su GY, Xu XQ, Zhou Y, Zhang H, Si Y, Shen MP, Wu FY (2021) Texture analysis of dual-phase contrast-enhanced CT in the diagnosis of cervical lymph node metastasis in patients with papillary thyroid cancer. Acta Radiol 62(7):890–896

20. Çaylaklı F, Yılmaz S, Özer C, Reyhan M (2015) The role of PET-CT in evaluation of cervical lymph node metastases in oral cavity squamous cell carcinomas. Turk Arch Otorhinolaryngol 53(2):67–72
21. Chaudhary S, Aher V, Birangane R (2015) Role of magnetic resonance imaging in the diagnosis of cervical lymph node metastasis with unknown primary. J Oral Maxillofac Radiol 3(3):97
22. Di Martino E, Nowak B, Krombach GA, Sellhaus B, Hausmann R, Cremerius U et al (2000) Ergebnisse der prätherapeutischen Lymphknotendiagnostik bei Kopf-Hals-Tumoren. Klinische Wertigkeit der 18FDG-Positronen-Emissions-Tomographie (PET) [Results of pretherapeutic lymph node diagnosis in head and neck tumors. Clinical value of 18-FDG positron emission tomography (PET)]. Laryngorhinootologie. 79(4):201–6
23. Bujoreanu I, Gupta V (2022) Anatomy, lymph nodes. In: StatPearls. StatPearls Publishing, Treasure Island (FL)
24. Piludu F, Marzi S, Ravanelli M, Pellini R, Covello R, Terrenato I, Farina D, Campora R, Ferrazzoli V, Vidiri A (2021) MRI-based radiomics to differentiate between benign and malignant parotid tumors with external validation. Front Oncol 11:656918
25. Rezaeian A, Ostovari M, Hoseini-Ghahfarokhi M, Khanbabaei H (2022) Diffusion-weighted magnetic resonance imaging at 1.5 T for peripheral zone prostate cancer: the influence of the b-value combination on the diagnostic performance of apparent diffusion coefficient. Pol J Radiol 87:e215–e219. https://doi.org/10.5114/pjr.115715
26. Norris CD, Quick SE, Parker JG, Koontz NA (2020) Diffusion MR imaging in the head and neck: principles and applications. Neuroimaging Clin N Am 30(3):261–282. https://doi.org/10.1016/j.nic.04.001
27. Suh CH, Choi YJ, Baek JH, Lee JH (2018) The diagnostic value of diffusion-weighted imaging in differentiating metastatic lymph nodes of head and neck squamous cell carcinoma: a systematic review and meta-analysis. AJNR Am J Neuroradiol 39(10):1889–1895
28. ElSaid NA, Nada OM, Habib YS, Semeisem AR, Khalifa NM (2014) Diagnostic accuracy of diffusion weighted MRI in cervical lymphadenopathy cases correlated with pathology results. Egypt J Radiol Nuclear Med 45(4):1115–1125
29. Li S, Cheng J, Zhang Y, Zhang Z (2015) Differentiation of benign and malignant lesions of the tongue by using diffusion-weighted MRI at 3.0 T. Dentomaxillofac Radiol 44(7):0325
30. Srinivasan A, Galban CJ, Johnson TD, Chenevert TL, Ross BD, Mukherji SK (2010) Utility of the k-means clustering algorithm in differentiating apparent diffusion coefficient values of benign and malignant neck pathologies. AJNR Am J Neuroradiol 31(4):736–740
31. Koh D-M, Collins DJ (2007) Diffusion-weighted MRI in the body: applications and challenges in oncology. Am J Roentgenol 188(6):1622–1635
32. Barchetti F, Pranno N, Giraldi G (2014) The role of 3 Tesla diffusion-weighted imaging in the differential diagnosis of benign versus malignant cervical lymph nodes in patients with head and neck squamous cell carcinoma. Biomed Res Int 2014:532095
33. Platzek I, Sieron D, Plodeck V, Borkowetz A, Laniado M, Hoffmann RT (2019) Chemical shift imaging for evaluation of adrenal masses: a systematic review and meta-analysis. Eur Radiol 29(2):806–817
34. Priola AM, Gned D, Veltri A, Priola SM (2016) Chemical shift and diffusion-weighted magnetic resonance imaging of the anterior mediastinum in oncology: current clinical applications in qualitative and quantitative assessment. Crit Rev Oncol Hematol 98:335–357
35. Winfeld M, Ahlawat S, Safdar N (2016) Utilization of chemical shift MRI in the diagnosis of disorders affecting pediatric bone marrow. Skeletal Radiol 45(9):1205–1212
36. Farshchian N, Tamari S, Farshchian N, Madani H, Rezaie M, Mohammadi-Motlagh HR (2011) Diagnostic value of chemical shift artifact in distinguishing benign lymphadenopathy. Eur J Radiol 80(2):594–597
37. Shetty A, Sipe AL, Zulfiqar M (2019) In-phase and opposed-phase imaging: applications of chemical shift and magnetic susceptibility in the chest and abdomen. Radiographics 39(1):115–135
38. Farshchian N, Tamari S, Farshchian N, Madani H, Rezaie M, Mohammadi-Motlagh HR (2011) Diagnostic value of chemical shift artifact in distinguishing benign lymphadenopathy. Eur J Radiol 80(2):594–597
39. Sungmin W, Jeong C, Youn KS, Hyup KS (2013) Adrenal adenoma and metastasis from clear cell renal cell carcinoma: can they be differentiated using standard MR techniques
40. Barchetti F, Pranno N, Giraldi G (2014) The role of 3 Tesla diffusion-weighted imaging in the differential diagnosis of benign versus malignant cervical lymph nodes in patients with head and neck squamous cell carcinoma. Biomed Res Int 2014:1–9
41. Global Cancer Observatory (2021) International Agency for Research on Cancer. World Health Organization. Accessed 06 June 2021
42. Gor DM, Langer JE, Loevner LA (2006) Imaging of cervical lymph nodes in head and neck cancer: the basics. Radiol Clin North Am 44(1):101–110
43. Surov A, Meyer HJ, Wienke A (2020) Apparent diffusion coefficient for distinguishing between malignant and benign lesions in the head and neck region: a systematic review and meta-analysis. Front Oncol 9:1362
44. Chung SR, Choi YJ, Suh CH, Lee JH, Baek JH (2019) Diffusion-weighted magnetic resonance imaging for predicting response to chemoradiation therapy for head and neck squamous cell carcinoma: a systematic review. Korean J Radiol 20(4):649–661
45. Zhang H, Zhang C, Zheng Z, Ye F, Liu Y, Zou S, Zhou C (2017) Chemical shift effect predicting lymph node status in rectal cancer using high-resolution MR imaging with node-for-node matched histopathological validation. Eur Radiol 27(9):3845–3855
46. Mittal P, Gupta R, Mittal A, Joshi S (2016) Chemical shift magnetic resonance imaging in differentiation of benign from malignant vertebral collapse in a rural tertiary care hospital in North India. J Neurosci Rural Pract 7(4):489–492

Publisher's Note